ORIGINAL PAPER

S. H. Withers · R. E. Peale · A. F. Schulte
G. Braunstein · K. M. Beck · W. P. Hess · R. J. Reeder

Broad distribution of crystal-field environments for Nd³⁺ in calcite

Abstract Calcite crystals were grown from solution with single-crystal dimensions up to 3 mm and doped up to $\sim$0.1 at% with Nd^{3+} ions. Phase purity was verified by powder X-ray diffraction. The concentration of Nd^{3+} was measured by energy-dispersive spectrometry and Rutherford backscattering spectrometry. Micro X-ray fluorescence mapping of the calcite grains indicates uniform Nd distribution in as-grown crystal grains. X-ray absorption fine structure suggests that Nd^{3+} is substituted for Ca^{2+} with local lattice distortion. Temperature-dependent near-infrared spectroscopy of Nd^{3+} impurities in calcite reveals large inhomogeneous linewidths and smooth line profiles that are characteristic of glassy hosts, though the samples are well crystallized.

Keywords Calcium carbonate · Calcite · Neodymium · Carbonate minerals · Nuclear waste

Introduction

Calcite ($CaCO_3$) is one of the most reactive mineral components in Earth's near-surface environment. It plays an important role in impurity sorption processes in soil and groundwater systems (Mecherri et al. 1990). The common occurrence of calcium carbonate at localities impacted by radionuclide waste has focused attention on the effectiveness of calcite in the sequestration of actinides. For example, carbonate minerals are present at the Hanford Nuclear Reservation in Eastern Washington State as grain coatings, particles, and as thick subsurface caliche layers (Slate 1996). Understanding of uptake processes, including adsorption and coprecipitation, and characterization of contaminants in carbonates are important for remediation efforts.

Calcite readily takes up divalent metal impurity ions in the Ca^{2+} site (Reeder et al. 1999), which is sixfold coordinated to O atoms of CO_3^{2-} groups. Uptake has been reported for ions much larger (e.g., Pb^{2+} and Ba^{2+}) and smaller (e.g., Co^{2+} and Zn^{2+}) than Ca^{2+} causing only local lattice distortions (Reeder et al. 2000). Less is known about heterovalent substitutions in calcite. Trivalent rare-earth elements (REEs) are strongly partitioned into calcite (Zhong and Mucci 1995), which suggests that calcite may play a strong role in determining their environmental fate. The uptake behavior of lanthanides is of particular interest because their chemical behavior is similar to that of the trivalent actinides (e.g., Pu^{3+}, Am^{3+}, Cm^{3+}). The latter group poses serious challenges for environmental remediation, yet, owing to its toxicity or radioactivity, it can be problematic for laboratory study.

This paper focuses on Nd^{3+} coprecipitated with calcite. Nd is usually considered the most important of the REEs from the environmental perspective because it is closest to Am^{3+} and Cm^{3+} in size. The ionic radius of Nd^{3+} (0.983 Å) is comparable to that of Ca^{2+} (1.00 Å) with sixfold coordination (Shannon 1976). The Ca site in calcite forms a nearly regular octahedron with all six Ca–O distances equal to 2.36 Å (Effenberger et al. 1981). Nd^{3+} is expected to occupy the Ca^{2+} site, as trivalent lanthanides are known to show a strong preference for substitution in Ca sites (Bünzli and Choppin 1989). Because calcite is essentially close-packed, the only other imaginable position for Nd^{3+} would be a defect site. Extended X-ray absorption fine structure (EXAFS) studies of the lanthanide series in synthetic calcite show

S. H. Withers · R. E. Peale (✉) · A. F. Schulte · G. Braunstein
University of Central Florida,
Department of Physics, Orlando, Florida 32816
e-mail: rep@physics.ucf.edu
Tel.: +407-823-3076
Fax: 407-823-5112

K. M. Beck · W. P. Hess
William R. Wiley Environmental Molecular Sciences Laboratory,
Pacific Northwest National Laboratory,
Richland, Washington

R. J. Reeder
Department of Geosciences,
Center for Environmental Molecular Science,
State University of New York,
Stony Brook, New York 11794-2100

that the local oxygen coordination changes from six- to seven-fold as the ionic radius increases (Elzinga et al., 2002), and the largest ion studied, Nd^{3+}, is sevenfold, which requires disruption of the local lattice structure. Possible mechanisms to account for the extra oxygen ligation have been suggested, including bidentate linkage of one carbonate group, or retention of an OH^- or H_2O from the REE hydration shell (Elzinga et al. 2002). Since increased coordination is observed only for larger trivalent REEs, it is unlikely that it can be attributed solely to the requirement of charge compensation. Hence, there remain fundamental scientific questions regarding Nd^{3+} in calcite.

Substitution of trivalent impurity ions for divalent host ions requires charge compensation since the host crystal must remain electrically neutral. Charge compensation is intimately related to the local structure surrounding the impurity, and it may involve local lattice distortion, defects, or other impurities. High-resolution low-temperature optical spectroscopy of Nd^{3+} heterovalently substituted for divalent ions in apatite crystals has revealed that the required charge compensation can occur in a wide variety of ways (Peale et al. 1995). The effect of charge compensation is revealed by shifts in optical transition frequencies (absorption and luminescence lines) caused by changes in the local crystal-field environment. Because defects and impurities occupy discrete lattice positions, an ensemble of densely grouped distinct lines, which can be isolated by site-selective photoluminescence, characterizes the spectra of these crystals. Occasionally, a smooth, generally weak background is also seen (Peale et al. 1995). The relative strength of the different contributions can depend strongly on REE concentration (Peale et al. 1995).

Though optical spectroscopies of some lanthanides and actinides in calcite have been reported (Mason and Mariano 1990; Piriou et al. 1997; Stumpf and Fanghänel 2002), the optical spectrum of Nd^{3+} in calcite has not been reported. In this paper, Nd^{3+} is introduced into calcite crystals by solution growth in order to learn about local site structure from optical spectroscopy. A considerable part of this paper is aimed at verifying the structure and doping of the solution-grown crystals.

Experimental

$CaCO_3$ crystals were grown from a room-temperature solution of 2% by mass $CaCl_2$ and 21% by mass NH_4Cl. Solid $(NH_4)_2CO_3$ was suspended above the solution in the headspace of the sealed reaction vessel. $CaCO_3$ forms after vapor diffusion of CO_2 and NH_3 into solution per the overall equation

$$CaCl_2 + (NH_4)_2CO_3 \Leftrightarrow CaCO_3 \downarrow + 2NH_4Cl \ ,$$

as described by Gruzensky (1967). The near steady-state breakdown of $(NH_4)_2CO_3$ allows growth of large calcite crystals, up to 3 mm in this case. Nd^{3+}-doped crystals were grown by the same method with 0.065% by mass $NdCl_3 \cdot 6H_2O$ added to the growth solution. Calcite crystals adhere to the vessel walls near the vapor–solution interface. Crystals were filtered from the growth solution after 30 days, thoroughly rinsed with deionized water, and dried in air. The as-grown crystal morphology was observed under a 45× stereo microscope.

The composition of the samples was characterized by Rutherford backscattering spectrometry (RBS) and by energy-dispersive spectrometry (EDS). RBS was performed using a 2.25 MeV alpha particle beam (1 mm diameter) on $Nd:CaCO_3$ pressed pellet samples (~10 μm rugosity). RBS signals arise from depths to a few 100 nm, so that beam penetration is much less than the crystal size (~100 μm). Data reduction was performed using the program RUMP (Doolittle 1985).

EDS spectra were measured by scanning a focused electron beam over an area on the surface of an as-grown single powder granule. No sample preparation was done to alter the surface of the grain, so that EDS (which is more sensitive to the surface than RBS) may have uncertainties related to surface irregularities. Such uncertainties arise because characteristic X-ray emission is attenuated to different degrees, depending on the path length within the sample (Scott and Love 1983).

Powder X-ray diffraction (Cu K_α radiation) was used to determine the crystal phase of the samples by comparison with database spectra using JADE (1995). Samples were ground in acetone with a mortar and pestle until relative diffraction peak intensities were repeatable after sample rearrangement.

Micro-X-ray fluorescence (μXRF) mapping was performed at the Advanced Photon Source (APS), PNC-CAT, beam line 20-ID at Argonne National Lab. Nd-doped calcite grains were mounted on high-purity silica glass slides and polished flat. The incident X-ray beam was focused to a 5×5-μm^2 spot that was rastered over the sample surface, which was positioned for 30° angle of incidence. Resultant Nd–L_α and Ca–K_α fluorescence were measured with a 13-element Ge detector positioned at 90° with respect to the incident X-ray beam.

EXAFS experiments were performed at beamlines 20-ID and 20-BM at the APS on the grown $Nd:CaCO_3$ and standard neodymium carbonate (Acros) $Nd_2(CO_3)_3 \cdot xH_2O$, respectively. Nd^{3+}-doped calcite samples were ground into fine powder and spread evenly onto clear tape. Nine layers were used to produce the desired edge step. Four layers of $Nd_2(CO_3)_3 \cdot xH_2O$ powder on Kapton tape were used. Si(111) monochromator crystals were used to produce a monochromatic beam, with one crystal detuned 25% to reduce harmonics. Nd L_3-edge (6.208 keV) fluorescence yield from $Nd:CaCO_3$ was measured with a 13-element Ge detector. $Nd_2(CO_3)_3 \cdot xH_2O$ L_3-edge spectra were measured using transmission methods.

EXAFS fits were performed using the program WinXAS (Ressler 1997) using theoretical phases and amplitudes calculated using the program FEFF6 (Rehr et al. 1992). The starting model for FEFF6 calculations assumed that Nd substituted in the Ca site of calcite. This has the Nd in octahedral coordination with no disruption of the local structure, though a significant disruption is suspected (Elzinga et al. 2002). The paths fitted extend to the Ca shell and not beyond.

Pressed pellets were made for most of the optical experiments discussed in this paper. Doped or undoped $CaCO_3$ was mixed with 10% by volume KBr and ground into fine powder. The powder was pressed into translucent disks at 10 000 psi to a thickness of 0.5 mm. Pressed pellets were made for control spectra by mixing 0.1 wt% $NdCl_3.6H_2O$ or 1 wt% $Nd_2(CO_3)_3 \cdot xH_2O$ with KBr.

Transmission spectroscopy was performed at the University of Central Florida using a Bomem DA8 Fourier spectrometer. Near-IR and visible transmittance measurements used a quartz-halogen lamp, quartz beam splitter, and an Si detector. Cooled InSb and HgCdTe detectors were used for transmittance measurements into the mid-IR. Mid-IR spectra were collected on synthetic calcite single crystals with ~mm dimensions and compared with spectra for plates of natural calcite. The sample thickness (mid-IR beam path) in each case was 300 μm. Low-temperature spectra were obtained using a CTI-cryogenics closed-cycle cooler with sample temperature monitored by a Si diode mounted on the copper cold finger. Samples were thermally contacted to the cold finger with rubber cement.

Near-IR fluorescence spectra were collected using a micro-spectroscopy setup with 488-nm excitation from an argon ion laser

(∼3 mW). As-grown samples were mounted on the *x*-*y*-*z* translation stage of a microscope and sampled with a long working distance 40× objective. The fluorescence was analyzed with a single-grating spectrograph (Instruments SA, HR 640) equipped with a CCD detector (Princeton Instruments). Low-temperature spectra were obtained using a small liquid-nitrogen cold finger cryostat. The wavelength scale was calibrated against five sharp $^4F_{3/2} \rightarrow ^4I_{9/2}$ luminescence lines from 2% Nd:SVAP (strontium fluorovanadate) at 80 K (Peale et al. 1995).

Results

The calcite crystals subsequently analyzed were scraped from the sides of the growth vessel. These crystals were large, opaque white rhombs and aggregates. A residue in the form of a very fine powder was also scraped off the bottom of the vessel, but was not analyzed for phase or composition. However, the faint purplish color of this residue suggests that it has a high Nd concentration compared with the calcite crystals.

The morphology of the as-grown undoped calcite crystals consists primarily of individual clear crystal rhombs with dimensions up to 3 mm. Some white spherical aggregates, consistent with previously reported vaterite morphology (Davies et al. 1978), were also identified. Nd^{3+}-doped crystals were slightly opaque and irregular, consisting of some large ∼2000-μm aggregates of acicular crystals, some smaller ∼100-μm multifaceted pieces, and other forms. Opacity is attributed to scattering on surface roughness, since the large undoped single crystals were observed to become perfectly transparent after polishing. No individual well-formed calcite rhombs were present in the doped material (see also Mason and Mariano 1990). However, characteristic 78° and 102° angles between facets were observed in some of the smaller crystals, which are consistent with the common (10$\bar{1}$4) calcite form, corresponding to perfect cleavage.

Rutherford backscattering

The RBS spectrum of Nd:CaCO$_3$ is shown in Fig. 1 (dots). Nd, Ca, O, and C signals are labeled. The Nd signal is slightly peaked at high energy, indicating a possibly higher Nd concentration on the surface layer (Czanderna and Hercules 1991). The line (Fig. 1) represents the simulated RBS spectrum created with RUMP (Doolittle 1985). Simulation parameters indicate an Nd concentration of 0.05 ± 0.01 at.% in the bulk of the Nd:CaCO$_3$ pellet, giving a composition Nd$_{0.0025}$Ca$_{0.9975}$CO$_3$, with twice that concentration at the surface.

The surface concentration might be an artifact due to decomposition of CaCO$_3$ into CaO and CO$_2$ during ion bombardment. A surface decrease in C or O would not be observed, since sensitivity to these elements is poor. Similarly, a surface increase in Ca due to decomposition would be less apparent than for Nd due to preferential sensitivity for high Z elements. Sensitivities are
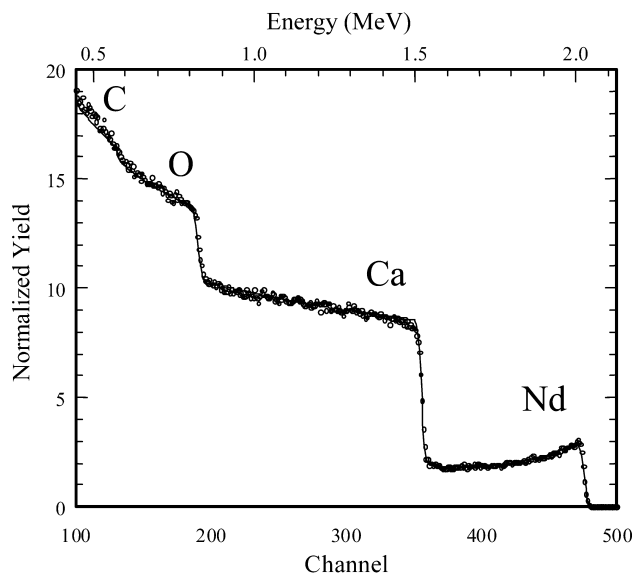

Fig. 1 Raw RBS spectrum (*dots*) and fitted spectrum (*line*) of Nd^{3+}:CaCO$_3$

1–10 at.% for Ca and 10–100 ppm for Nd, so that a 0.05 at.% increase in Ca would not show up at all.

Energy-dispersive spectrometry

The EDS fluorescence spectrum of Nd:CaCO$_3$ is shown in Fig. 2. X-ray fluorescence peaks from the sample are present for Ca, C, O, and Nd. A weak Al peak appears as an artifact from the sample holder. The C peak may be slightly enhanced since the sample was mounted with conductive carbon tape. The small Cl peak may indicate the presence of some residue on the sample surface or a Cl impurity. However, a residue is unlikely since the samples were thoroughly rinsed with deionized water. The Nd concentration was determined from normalized *k*-ratios of Nd-L$_\alpha$ and Ca-K$_\alpha$ characteristic X-ray peak
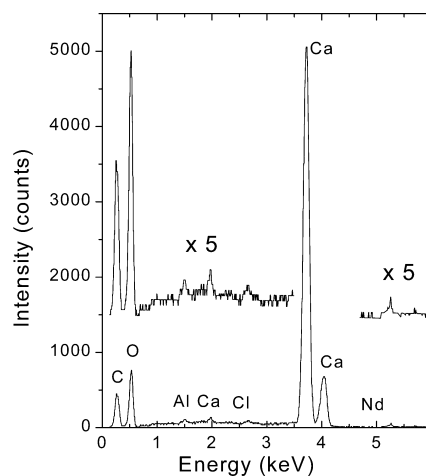

Fig. 2 EDS spectrum of Nd^{3+}:CaCO$_3$

intensities using a standardless ZAF corrected (Scott and Love 1983) quantitative analysis. Concentration information from this spectrum was averaged with two others giving [Nd] = 0.18 ± 0.02 at% (or $Nd_{0.009}Ca_{0.991}CO_3$). That this value exceeds that determined from RBS might be attributed to the comparatively high sensitivity of EDS to the surface, which may undergo some decomposition under electron bombardment.

Powder X-ray diffraction

Figure 3 shows the powder X-ray diffraction spectrum for (Fig. 3a) Nd doped samples and undoped (Fig. 3b) synthetic $CaCO_3$ crystals. These data have been normalized to the high-intensity ($10\bar{1}4$) reflection at 29.4° (Cu K_{α} radiation) and scaled to reveal details of low-intensity data. The two spectra have almost identical features, which correlate with reference powder diffraction data (Swanson et al. 1953) for calcite ($R\bar{3}c$) shown in Fig. 3c. There is no evidence of other $CaCO_3$ phases in (Fig. 3a) or for residual $NdCl_3$. In the undoped sample, there are six small peaks ∼85 times smaller than the main calcite peak in Fig. 3b at 21.1°, 25.1°, 27.2°, 32.9°, 43.9°, and 50.2° (indicated by arrows). These peaks indi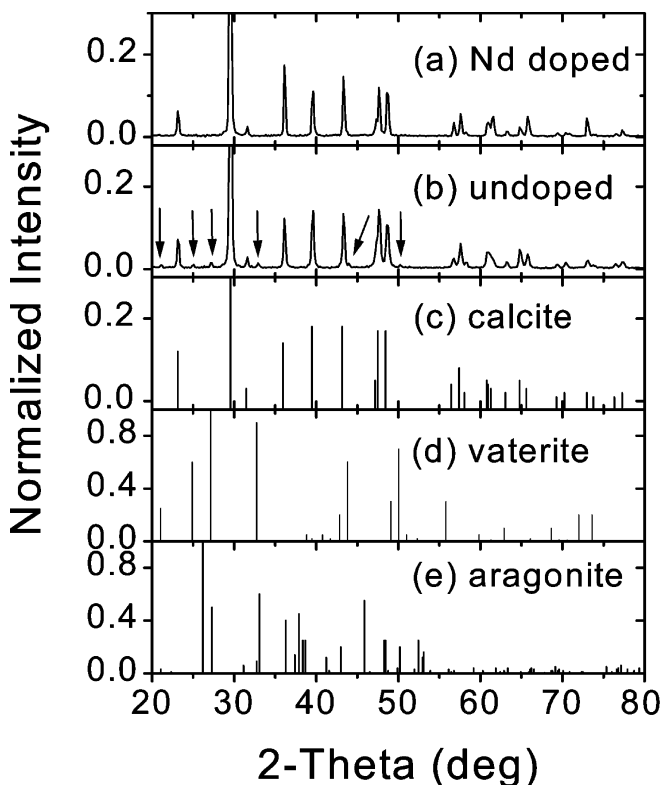cate traces of vaterite, a metastable polymorph of $CaCO_3$, whose reference powder diffraction spectrum (Rouse 1980) is shown in Fig. 3d. Spherical aggregates of vaterite were produced during the growth of undoped calcite, causing some phase contamination. Aragonite is another common, though metastable phase of $CaCO_3$ that is known to form at room temperature and atmospheric pressure (Togari and Togari 1955), but there is no evidence of the aragonite phase in Fig. 3a,b. Reference powder diffraction data (Keller et al. 1989) for aragonite (*Pmcn*) are shown in Fig. 3e.

Micro X-ray fluorescence

The ratio of Nd–L_{α} (5.230 keV) to Ca-K_{α} (3.691 keV) X-ray fluorescence is shown in the μXRF image in Fig. 4a, where lighter areas indicate higher ratio values. The calcite grain shown is approximately 650 μm across the bottom edge and 210 μm thick. The high Nd/Ca values (> 0.4) compared with relative concentrations from RBS (0.05 at% or [Nd]/[Ca] ∼ 0.0025) is due to the much higher fluorescence yield of Nd relative to Ca. The bright regions near step edges on the left and the dark region along the right of the sample are edge effects. Anomalous edge effects in XRF are common and can have multiple causes including the difference in absorption of the emitted X-rays and the geometry of the edge itself.

EXAFS spectroscopy

Fig. 5 shows a comparison of the k^3-weighted EXAFS spectra of $Nd:CaCO_3$ (light) and $Nd_2(CO_3)_3 \cdot xH_2O$

Fig. 3 The normalized powder x-ray diffraction spectra of *a* synthetic Nd:CaCO$_3$; *b* synthetic undoped CaCO$_3$; *c* reference data for calcite (Swanson and Tatge 1953); *d* reference data for vaterite (Rouse 1980); *e* reference data for aragonite (Keller et al. 1989)
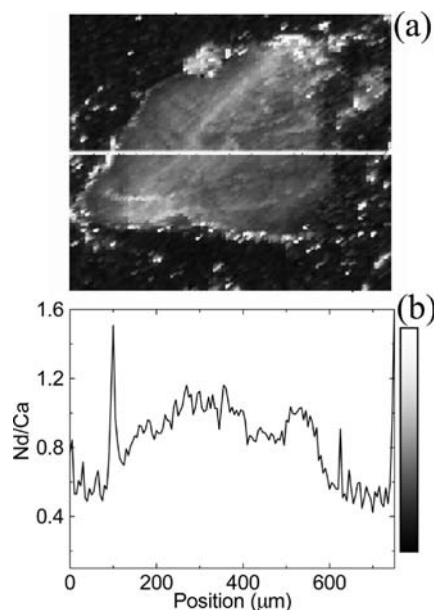

Fig. 4 a μXRF map of the Nd/Ca fluorescence ratio from a single polished calcite grain. *Lighter areas* indicate higher Nd concentration. The image is 750 μm wide and 850 μm high. **b** An intensity profile corresponding to the slice indicated in **a**
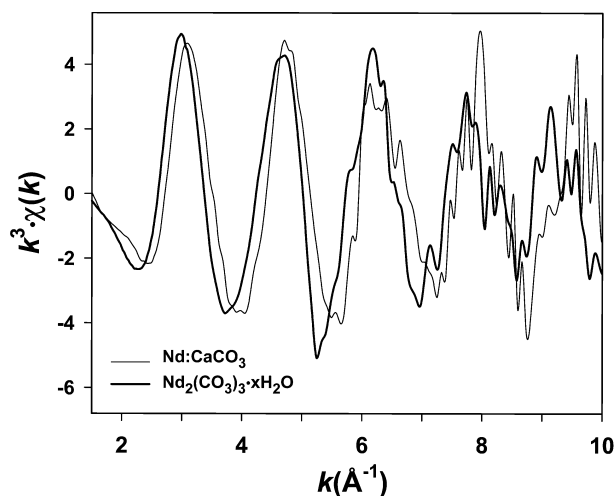
Fig. 5 The k^3-weighted $\chi(k)$ spectra for Nd^{3+}:$CaCO_3$ (*light*) and $Nd_2(CO_3)_3 \cdot xH_2O$ (*heavy*)

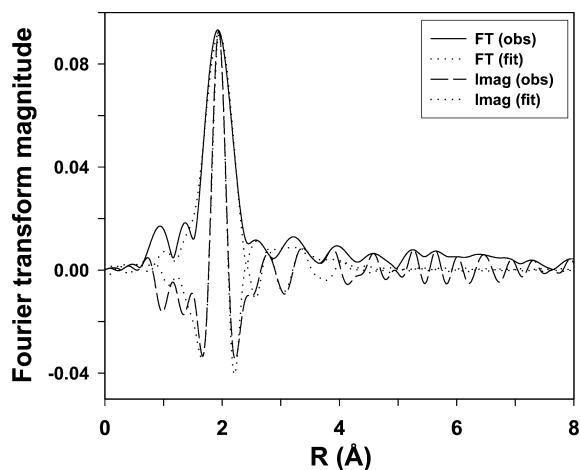**Fig. 6** The real and imaginary components of the Fourier transform of the k^3-weighted Nd L_3 edge EXAFS spectrum of Nd^{3+}:$CaCO_3$ and corresponding fits

(heavy) after background subtraction, normalization, and conversion to k-space. $Nd_2(CO_3)_3 \cdot xH_2O$ has slightly higher-frequency oscillations than $Nd:CaCO_3$, corresponding to a larger first-shell radius.

The heavy line in Fig. 6 is the Fourier transform magnitude of the k^3-weighted data from Fig. 5 for the $Nd:CaCO_3$ sample. The small peak at low R is an artifact from background subtraction. The dotted line in Fig. 6 shows the best fit using four scattering shells and assuming that Nd^{3+} occupies the Ca^{2+} site in calcite.

Single scattering events from the first ($Nd-O_1$), second ($Nd-C$), third ($Nd-O_2$), and fourth ($Nd-Ca$) atomic shells were considered. Fitting results are collected in Table 1. The data and corresponding fit give an average first shell ($Nd-O_1$) radius of 2.43 ± 0.02 Å and a coordination number of 6.6 ± 1. Higher-order shells were assigned a sixfold coordination corresponding to the ideal calcite structure. Fitting results indicate a second-shell ($Nd-C$) radius of 3.24 ± 0.04 Å, third-shell ($Nd-O_2$) radius 3.51 ± 0.04 Å, and fourth-shell ($Nd-Ca$) radius 4.25 ± 0.04 Å. The corresponding shell radii in an ideal calcite structure are 2.36 Å ($Ca-O_1$), 3.21 Å ($Ca-C$), 3.46 Å ($Ca-O_2$), and 4.04 Å ($Ca-Ca$), indicating substantial lattice dilation around the Nd^{3+} impurity. Inconsistencies between the fitted and observed spectra in the range of the C and O_2 shells and the large Debye–Waller factors for these more distant shells suggest that the local coordination exhibits some differences from the ideal calcite structure.

Near-infrared absorption

Figure 7 shows the $^4I_{9/2} \rightarrow {}^4F_{3/2}$ absorption band for $Nd:CaCO_3$ at 300, 90, and 8 K. There is some line sharpening as the sample is cooled from 300 to 90 K, but no further change is observed in the spectra as it is cooled to 8 K. The $^4G_{5/2} + {}^2G_{7/2}$ and $^2K_{13/2} + {}^4G_{7/2}$ absorption bands were also observed in the upper visible, and the $^4I_{13/2}$ and $^4I_{15/2}$ bands were observed in the mid-IR with only moderate interference from calcite lattice bands. Lattice bands obscured the $^4I_{11/2}$ band. In all bands, the same temperature dependence was observed.

Absorption spectra of model compounds were measured to test the question whether the observed absorption lines arise from Nd^{3+} actually in calcite or from a second phase, such as $Nd_2(CO_3)_3$, or as a residue of $NdCl_3$ on the crystal surface (though not detected in powder XRD, Fig. 3a). Figure 8 compares the 8 K $NdCl_3.6H_2O$, $Nd_2(CO_3)_3$, and $Nd:CaCO_3$ pressed pellet spectra, which are seen to differ substantially in width, position, and number of lines. The $^4F_{5/2} + {}^2H_{9/2}$ and $^4F_{7/2} + {}^4S_{3/2}$ bands were also observed to differ markedly for the two samples.

Micro photoluminescence

Though pellet absorption spectra of $Nd:CaCO_3$ and $Nd_2(CO_3)_3 \cdot xH_2O$ differ, they are similar enough to motivate additional comparison. Nd^{3+} fluorescence was

Table 1 EXAFS fitting parameters for Nd^{3+}: $CaCO_3$. The amplitude reduction factor S_0^2 was fixed at 1. A global threshold energy E_0 was refined (4.90 eV)

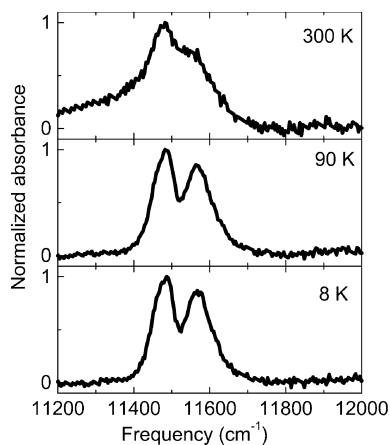| Shell	Coordination number (CN)	Shell radius R(Å)	Debye–Waller factor σ^2 (Å^2)
Nd–O	6.6 ± 1	2.43 ± 0.02	0.006 ± 0.002
Nd–C	6 (fixed)	3.24 ± 0.04	0.013 ± 0.002
Nd–O	6 (fixed)	3.51 ± 0.04	0.018 ± 0.002
Nd–Ca	6 (fixed)	4.25 ± 0.04	0.026 ± 0.002

Fig. 7 Near-IR pellet absorption spectra of $^4I_{9/2} \rightarrow {}^4F_{3/2}$ transitions in Nd:CaCO$_3$ at 300, 90, and 8 K

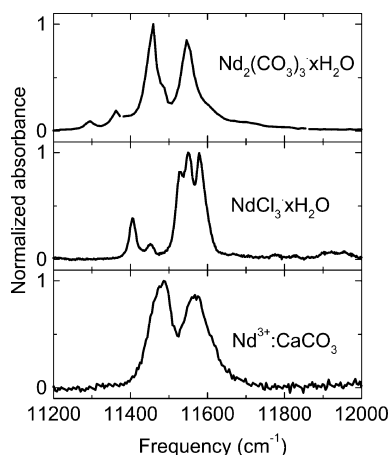**Fig. 9** Near-IR fluorescence spectra of $^4F_{3/2} \rightarrow {}^4I_{9/2}$ transitions at 90 K in Nd:CaCO$_3$ and Nd$_2$(CO$_3$)$_3 \cdot x$H$_2$O

Fig. 8 Near-IR pellet absorption spectra of Nd^{3+} in Nd:CaCO$_3$, Nd$_2$(CO$_3$)$_3 \cdot x$H$_2$O, and NdCl$_3$·6H$_2$O at 8 K
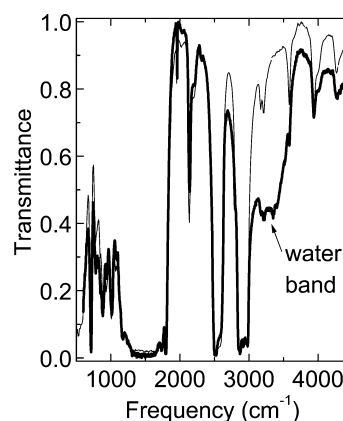
Fig. 10 Mid-IR transmittance spectra of synthetic (*heavy*) and natural (*light*) calcite samples

measured with a micro-Raman spectroscopy setup in order to allow measurement of low fluorescence yields from individual as-grown crystal grains. This reduces the averaging over grains that occurs in pellet spectra. Fig. 9(a) shows the Nd^{3+} $^4F_{3/2} \rightarrow {}^4I_{9/2}$ transitions from a Nd:CaCO$_3$ crystal aggregate ($\sim$1200 µm) at 90 K. This spectrum is typical of all samples measured, aside from differences in noise level and counting rate, which were correlated to the grain size. The smallest sample measured successfully was a single $\sim$400-µm grain. The line shape appears to be independent of the number of grains excited. Figure 9b shows the same Nd^{3+} transition in Nd^2(CO$_3$)$_3 \cdot x$H$_2$O. The spectral differences in the number of lines and line widths between these two samples are even stronger than in the absorption data.

Mid-IR spectroscopy

A comparison of mid-IR absorption spectra for a natural calcite sample (light) and an undoped solution-grown calcite rhomb (heavy) is shown in Fig. 10. The 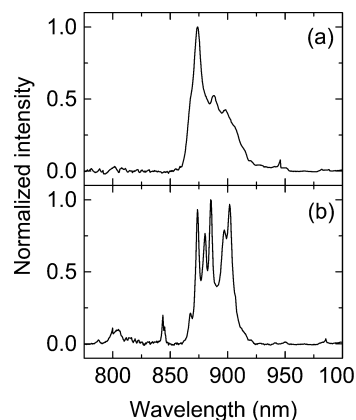usual calcite lattice bands have nearly equal strength for the two samples. The synthetic crystal has a strong water absorption band centered at 3300 cm^{-1} (Robinson 1974). This band is absent (or much weaker) in the natural calcite spectrum.

Discussion

Calcite phase purity was verified by powder X-ray diffraction, and the sharp X-ray lines show that it is well crystallized. However, a second Nd-containing phase might go undetected by X-ray diffraction if present below 1%. Meinrath and Takeishi (1993) studied the precipitation of Nd^{3+} phases in the Nd^{3+}–CO$_2$–H$_2$O system at 25 °C in low ionic strength solutions. At CO$_2$ partial pressures of $10^{-3.5}$ atm, the initial precipitate was observed to be Nd$_2$(CO$_3$)$_3 \cdot x$H$_2$O ($x = 4.5$–6). This precipitate transformed to NdOHCO$_3$ after aging for 30 days. The hydroxycarbonate was considered to be the solubility-limiting phase at low CO$_2$ partial pressure. Carroll (1993) studied Nd^{3+} precipitation in calcite- and/or Ca^{2+}-containing systems at 25 °C and CO$_2$ partial pressures of 0.05–0.3 atm. She observed

formation of a Nd–Ca carbonate phase, which was interpreted as having the orthorhombic $NdOHCO_3$ structure. Solutions were not supersaturated with respect to calcite, and there was no indication that Nd^{3+} coprecipitated with calcite.

In the $NdOHCO_3$ structure, Nd^{3+} is in ninefold coordination with oxygens and the average Nd–O distance is 2.598 Å (Dexpert and Caro 1974). This Nd–O distance is significantly greater than the distance determined by EXAFS for our Nd-containing calcite (2.43 Å), and so we rule that out as a significant second phase in our calcite. In view of the findings of Carroll (1993), a mixed Ca–Nd hydroxycarbonate with the $NdOHCO_3$ structure could form. Although structural information and composition of such a phase is unknown, Nd–O coordination and distances should be similar to those in $NdOHCO_3$ if it is isostructural. Such a Ca–Nd hydroxycarbonate is inconsistent with EXAFS observations on our calcite sample.

The structure of $Nd_2(CO_3)_3 \cdot xH_2O$ has not been reported; however, comparison of the EXAFS spectrum for $Nd_2(CO_3)_3 \cdot xH_2O$ with our Nd-containing calcite (Fig. 5) shows that this phase is also not an impurity. There are also clear differences in the number of lines, line width, and center frequency in near-IR absorption and fluorescence spectra between our Nd-doped calcite samples and $Nd_2(CO_3)_3 \cdot xH_2O$ (as well as $NdCl_3.6H_2O$). Mapping by μXRF indicates a fairly uniform distribution of Nd in the as-grown crystal grains, which would be unlikely if the Nd were concentrated in a second phase. Hence, EXAFS, μXRF, and optical measurements support the conclusion that Nd^{3+} signals in our samples originate from Nd^{3+} in calcite, not other phases.

EXAFS analysis of $Nd:CaCO_3$ shows that the local lattice distortion is substantial. EXAFS supports the conclusion that Nd is substitutional for Ca in calcite, but with an increase in first-shell (Nd–O) radius and coordination, as well as some lattice dilation in the second and third coordination shells. Other studies of lanthanide impurities in calcite are consistent with this result, reporting sixfold coordination for the smaller lanthanides Dy and Yb and sevenfold coordination for the larger lanthanides Nd and Sm (Elzinga et al. 2002). Possible mechanisms whereby an additional oxygen atom is incorporated within the first coordination shell have been proposed (Elzinga et al. 2002). The same effect is absent in smaller trivalent REEs, suggesting a disparity in the charge compensation mechanism across the lanthanide series.

The large line width and absence of line sharpening below 90 K for the near-IR absorption spectra indicate a high degree of inhomogeneous broadening. In other charge-compensated Nd-doped crystals, such as melt-grown Nd:strontium fluoroapatite (Fig. 11) (Peale et al. 1995), where different crystal-field environments give rise to discrete lines that can be more or less resolved, line widths at 300 K are tens of cm^{-1}, decrease to a few cm^{-1} at liquid nitrogen temperature, and can decrease further
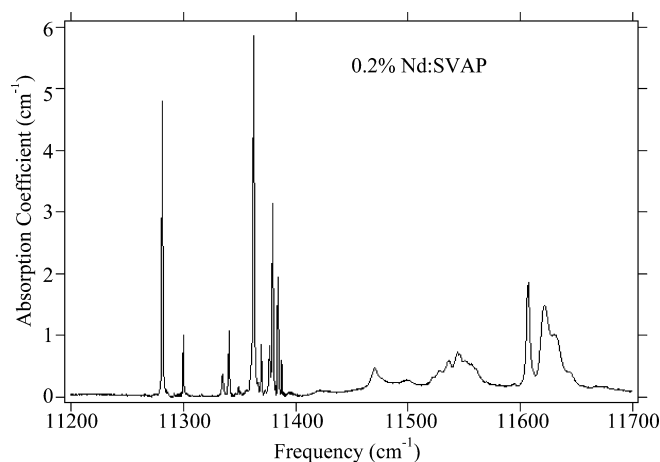

Fig. 11 $^4I_{9/2} \rightarrow ^4F_{3/2}$ absorption spectrum of Nd:SVAP at 2 K. (Peale et al. 1995)

even to sub-cm^{-1} widths at liquid helium temperature (Hong et al. 1995). Discrete lattice effects dominate the Nd:SVAP spectrum (Fig. 11) with only a weak continuous background. In contrast, although the usual two $^4F_{3/2}$ lines are seen in Fig. 7, each has a temperature-independent width of ∼80 cm^{-1} below 90 K. Because the lines are smooth, without discrete structure, one may infer that the very large widths result from a broad and continuous distribution of crystal-field environments. As Fig. 11 shows, a distribution of discrete center frequencies, spanning several 100 cm^{-1} in charge-compensated Nd^{3+} doped crystals, is not unusual, but the smoothness of this distribution in calcite is more characteristic of glassy (Mann and DeShazer 1970) than crystalline hosts. Yet the powder X-ray diffraction shows that our samples are well-crystallized. The apparent independence of sample size of the microphotoluminescence line shapes shows that the broad line widths come from a distribution within individual grains and not among grains.

Dieke (1968) reports that broad absorption lines, such as those for $Nd:CaCO_3$, have been observed repeatedly from rare-earth ions in solution-grown crystals, and he attributes the broadening to nonuniform lattice strain. Lattice strain induced by incorporation of molecular H_2O may contribute to the broadening of Nd^{3+} lines. Mid-IR spectra (Fig. 10) reveal strong water-related absorption bands in solution-grown crystals that are absent in a natural calcite sample. This may reflect structurally bound H_2O, although liquid water could also be present in fluid inclusions. Broad Nd^{3+} absorption lines are also observed in the absorption spectra of the two reference compounds (Fig. 9a) $NdCl_3.6H_2O$ and $Nd_2(CO_3)_3 \cdot xH_2O$ with approximate linewidths at 8 K of 25 and 40 cm^{-1} respectively, while $Nd:CaCO_3$ has linewidths of 80 cm^{-1}. Since these two hydrophilic reference compounds are likely to be variably hydrated and to a higher degree than $Nd:CaCO_3$, yet their line widths are less, the high degree of broadening observed in our samples is difficult to explain by hydration-induced lattice strain alone.

Hydroxylation of Nd^{3+} in the Ca^{2+} site is a likely possibility. The extra oxygen in the first shell of Nd^{3+} (needed to explain the lattice distortion found by EXAFS) could arise from a hydroxyl ion bound to the Nd. In a study of Eu^{3+} coprecipitation with calcite, Stipp et al. (2003) proposed that $EuOH^{2+}$ substitutes for Ca^{2+}, which satisfies charge balance. If OH^- were incorporated with the Nd^{3+}, while still retaining six oxygen ligands from CO_3 groups, it would satisfy charge compensation as well as the additional oxygen ligation indicated by the EXAFS. We note that aqueous speciation calculations for Nd^{3+} in calcite-saturated solutions indicate that the $NdOH^{2+}$ species is nearly two orders of magnitude lower in concentration than $NdCO_3^+$ and $Nd(CO_3)_2^-$. Nevertheless, it is possible that, once adsorbed at the surface, Nd^{3+} becomes hydroxylated, as suggested by Stipp et al. (2003) for Eu^{3+}, and $NdOH^{2+}$ becomes incorporated into the growing calcite.

It is worth comparing the results in this study to previous optical investigations of rare-earth ions in calcite. Piriou et al. (1997) studied sorption of Eu on natural calcite, where a minority of Eu was determined to occupy Ca^{2+} sites, the majority going into other phases. The present paper studies coprecipitation of Nd in synthetic calcite, and the interpretation is that the majority of Nd goes into substitutional Ca^{2+} sites. Secondary phases were also identified in our growth vessel, but evidence from physical characterization suggests these were unassociated with the calcite crystals and were easily separated. Additional adsorbed or surface-precipitated phases, such as observed by Pirou et al. (1997), are further discounted in our samples due to ongoing crystallization in our growth chamber, the small surface areas of our crystals, and the postgrowth rinsing.

The low-temperature linewidths in the spectra of substitutional Eu from Piriou et al. (1997) are about $\sim 50\ cm^{-1}$, which is still very broad compared to those observed in Eu-doped melt-grown crystals. Hence, though charge compensation and lattice distortions are not discussed by Piriou et al. (1997), the substitution of Eu^{3+} in the Ca^{2+} site is not simple (i.e., more complex than a unique crystal field). However, it is intriguing that the Eu^{3+} lines are narrower than we find for Nd^{3+}. One might expect that if both Eu^{3+} and Nd^{3+} occupied a bulk Ca site with the normal sixfold coordination, their line widths would be more similar. However, independent evidence (Elzinga et al. 2002) suggests that Nd (and Sm) have higher than sixfold coordination, indicating a defect-type site, so the larger line width for Nd over Eu is understandable. In contrast to Nd and Sm, the smaller Dy and Yb have sixfold coordination, and somewhere between the two groups, a cross-over is expected. The position of Eu in the Periodic Table is intermediate. Its comparatively narrow line width suggests it belongs to the sixfold group.

Implications may be drawn from this study of $Nd:CaCO_3$ regarding long-term retention or remobilization of Nd^{3+}-like ions from calcite minerals. The incorporation of Nd in calcite with substantial lattice dilation indicates large local strain. This implies an increase in Gibbs free energy and higher dissolution rate. This assertion is supported by simulations of crystal dissolution (Lasaga et al. 2001), which show that defect centers may act as dissolution nucleation sites on mineral surfaces. At high undersaturation conditions, these nucleation sites develop into etch pits with emanating dissolution stepwaves that extend over the crystal surface, causing global dissolution (Lasaga et al. 2001).

We end this paper by making some testable hypotheses. The strain field associated with Nd^{3+} ions in calcite should cause etch pit formation and increase the overall mineral dissolution rate. The actinide species Pu^{3+}, Am^{3+}, and Cm^{3+} are likely to exhibit similar behavior since they have the same valence and similar ionic radii as Nd^{3+}. The Nd^{3+}-like REEs are more likely to remobilize than REEs that cause less disruption of the local coordination in calcite. We further hypothesize that the coordination number of Eu^{3+} in calcite is six.

References

Bünzli J-CG, Choppin GR (eds) (1989) Lanthanide probes in life, chemical and Earth sciences. Elsevier Science New York

Carroll SA (1993) Precipitation of Nd–Ca carbonate solid solution at 25 °C. Geochim Cosmochim Acta 57: 3383–3393

Czanderna AW, Hercules DM (eds) (1991) Ion spectroscopies for surface analysis. Plenum, New York

Davies P, Dollimore D, Heal GR (1978) Polymorph transition kinetics by DTA. J Therm Anal 13(3): 473–487

Dieke GH (1968) Spectra and energy levels of rare-earth ions in crystals. Wiley, New York

Doolittle LR (1985) Algorithms for the rapid simulation of Rutherford backscattering spectra. Nucl Instrum Meth (B) 9(3): 344–351

Dexpert H, Caro P (1974) Determination de la structure cristalline de la variété à des hydroxycarbonates de terres rares LnOHCO$_3$. Mat Res Bull 9: 1577–1586

Effenberger H, Mereiter K, Zemann J (1981) Crystal-structure refinements of magnesite, calcite, rhodochrosite, siderite, smithonite, and dolomite, with discussion of some aspects of the stereochemistry of calcite-type carbonates. Z Kristallogr 156(3–4): 233–243

Elzinga EJ, Reeder RJ, Withers SH, Peale RE, Mason RA, Beck KM, Hess WP (2002) XAFS study of rare earth element coordination in calcite. Geochim Cosmochim Acta 66: 2875–2885

Gruzensky PM (1967) Growth of calcite crystals. In: Peiser HS (ed) Proceedings of the International Conference on Crystal Growth (Boston, 20–24 June 1966), Pergamon, New York, pp 365–367

Hong P, Zhang XX, Peale RE, Weidner H, Bass M, Chai BHT (1995) Spectroscopic characteristics of Nd^{3+}-doped strontium fluorovanadate and their relationship to laser performance. J Appl Phys 77(1): 294–300

448

JADE for Windows V3.1 XRD Pattern processing for the PC (1995) (Computer Software). Materials Data, Inc, Livermore, CA.

Keller L, Rask J, Buseck P (1989) Arizona State Univ., Tempe, AZ, USA, PDF#41-1475. Retrieved from JADE for Windows V3.1 Powder Diffraction File

Lasaga AC, Luttge A (2001) Variation of crystal dissolution rate based on a stepwave Model. Science 291: 2400

Mann MM, DeShazer LG (1970) Energy levels and spectral broadening of neodymium ion in laser glass. J Appl Phys 41: 2951–2957

Mason RA, Mariano AN (1990) Cathodoluminescence activation in manganese-bearing and rare-earth-bearing synthetic calcites. Chem Geol 88: 191–206

Mecherri OM, Budiman-Sastrowardoyo P, Rouchaud JC, Fedoroff M (1990) Study of neodymium sorption on orthose and calcite for radionuclide migration modelling in groundwater. Radiochim Acta 50: 169–175

Meinrath G, Takeishi H (1993) Solid–liquid equilibria of Nd^{3+} in carbonate solutions. J Alloys Compounds 194: 93–99

Peale RE, Summers PL, Weidner H, Chai BHT, Morrison CA (1995) Site-selective spectroscopy and crystal-field analysis for Nd^{3+} in strontium fluorovanadate. J Appl Phys 77(1): 270–276

Piriou B, Fedoroff M, Jeanjean J, Bercis L (1997) Characterization of the sorption of europium(III) on calcite by site-selective and time-resolved luminescence spectroscopy. J Colloid Interface Sci 194: 440–447

Reeder RJ, Lamble GM, Northrup PA (1999) XAFS study of the coordination and local relaxation around Co^{2+}, Zn^{2+}, Pb^{2+}, and Ba^{2+} trace elements. Am Mineral 84(7–8): 1049–1060

Reeder RJ, Nugent M, Lamble GM, Tait CD, Morris DE (2000) Uranyl incorporation into calcite and aragonite: XAFS and luminescence studies. Environ Sci Technol 34(4): 638–644

Rehr JJ, Zabinsky SI, Albers RC (1992) High-order multiple-scattering calculations of X-ray-absorption fine-structure. Phys Rev Lett 69(23): 3397–3400

Ressler T (1997) WinXAS: a new software package not only for the analysis of energy-dispersive XAS data. J Phys IV 7(C2): 269–270

Robinson JW (ed) (1974) Handbook of spectroscopy v II, CRC Press, Cleveland, p 78

Rouse R (1980) Dept. of Geological Sciences, Univ. of Michigan, Ann Arbor, MI, USA, PDF#33–0268. Retrieved from JADE for Windows V3.1 Powder Diffraction File

Scott VD, Love G (1983) Quantitative electron-probe microanalysis, Wiley, New York

Shannon RD (1976) Revised effective ionic-radii and systematic studies of interatomic distances in halides and chalcogenides. Acta Crystallogr (A) 32: 751–767

Slate JL (1996) Buried carbonate paleosols developed in Pliocene-Pleistocene deposits of the Pasco Basin, south-central Washington, USA. Quaternay International, 34–36, 191–196

Stipp SLS, Lakshtanov LZ, Jensen JT, Baker JA (2003) Eu^{3+} uptake by calcite: preliminary results from coprecipitation experiments and observations with surface–sensitive techniques. J Contaminant Hydrol 61: 33–43

Stumpf T Fanghänel T (2002) A time-resolved laser fluorescence spectroscopy (TRLFS) study of the interaction of trivalent actinides [Cm(III)] with calcite. J Coloid Interface Sci 249: 119–122

Swanson HE, Fuyat RK, Tatge E (1953) Natl. Bur. Stand. (US), Circ. 539, II 51, PDF#05–0586. Retrieved from JADE for Windows V3.1 Powder Diffraction File

Togari K, Togari S (1955) Conditions controlling the crystal form of calcium carbonate minerals. J Fac Sci Hokkaido Univ Ser 4 Geology and Mineralogy 9: 55–65

Zhong S, Mucci A (1995) Partitioning of rare-earth elements (REEs) between calcite and seawater solutions at 25 °C and 1 atm, and high dissolved REE concentrations. Geochim Cosmochim Acta 59: 443–453